Efficient inverted FA–Cs perovskite solar modules fabricated by blade-coating on PET foils with robust encapsulation

Anna Wąsiak-Maciejak[a,b], Mateusz Ścigaj[a], Klaas Bakker[c], Dorrit Roosen-Melsen[c], Łukasz Przypis[a,d,e], Konrad Dyk[a], Patrycja Janicka[f], Kinga Rycek[f], Daimiota Takhellambam[b], Aldo Di Carlo[b,g], and Konrad Wojciechowski*[a,d,e]

[a.] *Saule Research Institute, Duńska 11, 54-427 Wrocław, Poland.*
[b.] *CHOSE – Centre for Hybrid and Organic Solar Energy, Department of Electronic Engineering, University of Rome ''Tor Vergata'', Via del Politecnico 1, 00133, Rome, Italy.*
[c.] *TNO, Netherlands Organisation for Applied Scientific Research, Solar Technologies and Applications, High Tech Campus 21, 5656AE, The Netherlands.*
[d.] *Department of Semiconductor Materials Engineering, Wroclaw University of Science and Technology, Wybrzeże Wyspiańskiego 27, 50-370 Wrocław, Poland.*
[e.] *Chemini, 1 Maja 92A, Rosnówko, 62-052 Komorniki, Poland.*
[f.] *Saule Technologies, Duńska 11, 54-427 Wrocław, Poland.*
[g.] *Istituto di Struttura della Materia- Consiglio Nazionale delle Ricerche Roma (ISM-CNR), 00133 Rome, Italy.*

Characterisation methods

Current -voltage (I-V) measurements of cells and unencapsulated modules
I-V measurements were conducted under simulated AM1.5G irradiation (100 mW/cm^2) using an AAA-rated solar simulator Sun 2000 from Abet Technologies, calibrated with an RR-208-KG5 silicon reference cell from Abet Technologies. The solar cells were masked to 0.09 cm².

Current -voltage (I-V) measurements of encapsulated modules
For damp heat stability testing, the I-V measurements of the modules were conducted under simulated AM1.5G irradiation (100 mW/cm^2) using the Neonsee solar simulator, calibrated with the Konika Minolta AK200 reference cell. Series and shunt resistances were extracted from the I-V curves at V_{OC} and $I_{SC,}$ respectively.

Bending test
Repeated bending cycle measurements were conducted using a custom-designed one-dimensional mobile platform powered by a stepper motor.

Damp heat test
A damp heat test was conducted in the climatic chamber Espec EGNX12-7.5 CWL.

Steady-state photoluminescence measurement (ss-PL)
Steady-state photoluminescence measurements were conducted using a hyperspectral imaging microscope from Photon Etc., equipped with a 532 nm wavelength green laser as the excitation source.

Ultraviolet-visible (UV-VIS) spectroscopy
UV-Vis absorption spectra were measured with the Edinburgh Instruments Spectrofluorometer FS5, using an Xe lamp light source.

Scanning electron microscopy (SEM)
SEM images were acquired using the Phenom Pro-X microscope.

X-ray diffraction measurement (XRD) of perovskite films
X-ray diffraction (XRD) diffractograms of perovskite thin films were obtained using the Rigaku MiniFlex diffractometer with the CuKα (λ = 1.541 Å) radiation with Ni filter and generator parameters V = 40kV, I = 15mA at room temperature. Scans were performed in the range 5-50° with a step size of 0.01°.

X-ray diffraction measurement (XRD) of delaminated modules
XRD (X-ray diffraction) measurements were collected in Bragg−Brentano configuration for 2θ ranges from 5° to 60° focusing the impinging beam with fixed divergent slits (1/4−1/2°). XRD measurements were performed in reflection mode on a Rigaku SmartLab diffractometer by means of Kα fluorescence lines (Kα1 [Å] = 1.54060; Kα2 [Å] = 1.54441) of a Cu anode. Continuous scan with a solid-state hybrid PIXcel3D detector, working in 1D linear mode, accomplished the detection.

Electroluminescence and photoluminescence (EL-PL)

For EL-PL characterization of modules, the GreatEye lumisolar system was used with a 750 nm long-pass filter in front of the camera, green (523 nm) LEDs, and an f/8 aperture. Start with 10 seconds of preconditioning at +40 mA. EL at 40 mA, PL open and short-circuited; adjust exposure so that an acceptable picture is obtained between 250 and 1000 ms.

Lock-in thermography (LIT)
LIT measurement was conducted with the Infratec PV-LIT system using green LEDs; lock-in frequency was 250 mHz, and the duration was 90s, both at open and short circuit.

Ellipsometry
Ellipsometry data were collected by a Semilab SE-2000 ellipsometer, using an illumination angle of 70 degrees, and a spectral range 320-827 nm. The following models were used for each material: TCO and NiOx - Tauc-Lorentz + Drude, Perovskite: 5 Tauc-Lorentz.

Synthesis of NiO_X

Synthesis of NiO_X nanoparticles. $Ni(NO_3)_2 \cdot 6H_2O$ (3 g) was dissolved in 60 mL of deionized water and stirred at room temperature to form a clear green solution. Sodium hydroxide solution was added dropwise under constant stirring until the pH reached 10, and stirring was continued for 10 minutes to age the green nickel hydroxide precipitate. The precipitated slurry was filtered and washed multiple times with deionized water and ethanol. The wet precipitate was dried overnight at 80°C and then calcined at 270°C for 30 minutes to yield dark-black NiO_X nanopowder ready for dispersion preparation and further processing.

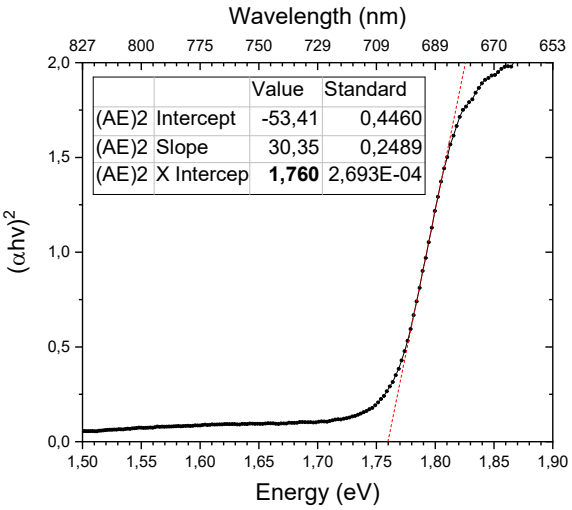

Figure S1. Tauc plot of WBG perovskite of composition $Cs_{0.2}FA_{0.8}Pb(I_{0.65}Br_{0.35})_3$.

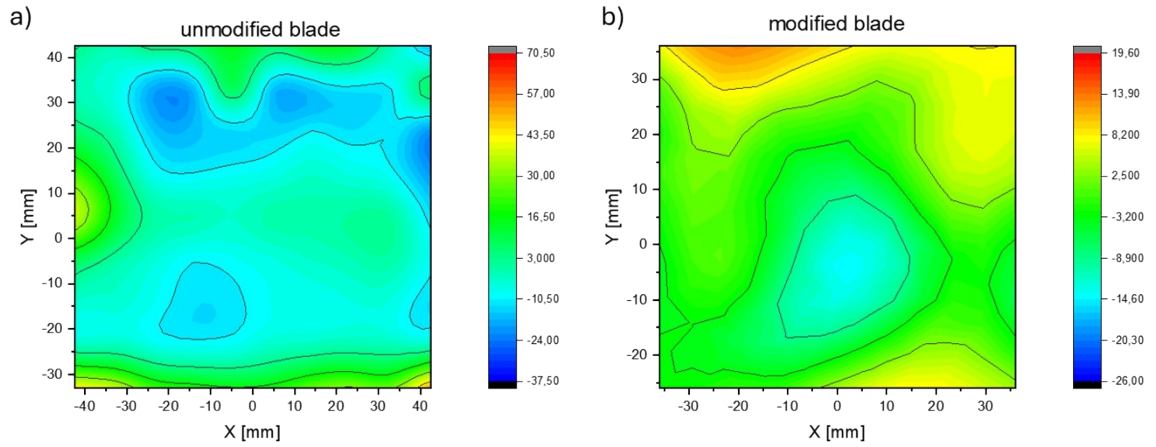

Figure S2. Spectroscopic ellipsometry thickness maps of WBG perovskite films: a) unmodified (without shielding element), b) modified blade (with shielding element). The color scale represents the relative deviation in thickness from the spatial mean, defined as $((t - \bar{t})/\bar{t}) \times 100\%$, where t is the local thickness and $\bar{t}$ is the mean thickness across the mapped area.

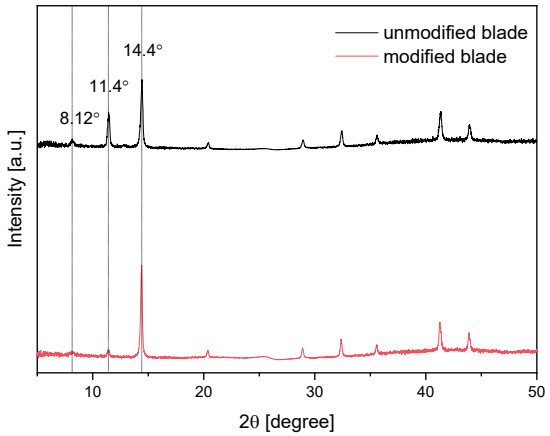

Figure S3. Impact of blade modification with shielding element on WBG perovskite films XRD diffractograms.

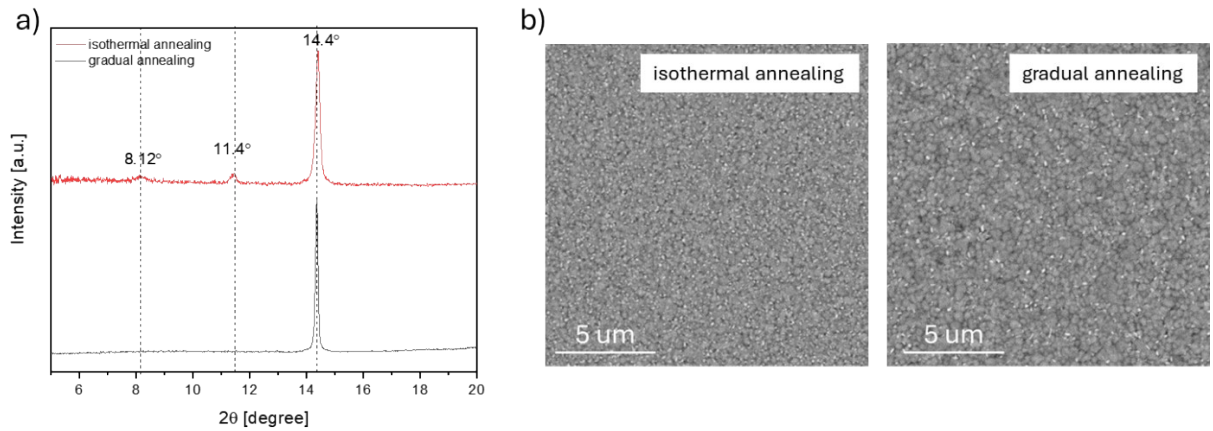

Figure S4. Impact of the annealing protocol on WBG perovskite film formation. Comparison between gradual and isothermal annealing conditions: a) XRD diffractograms of the resulting perovskite layers,

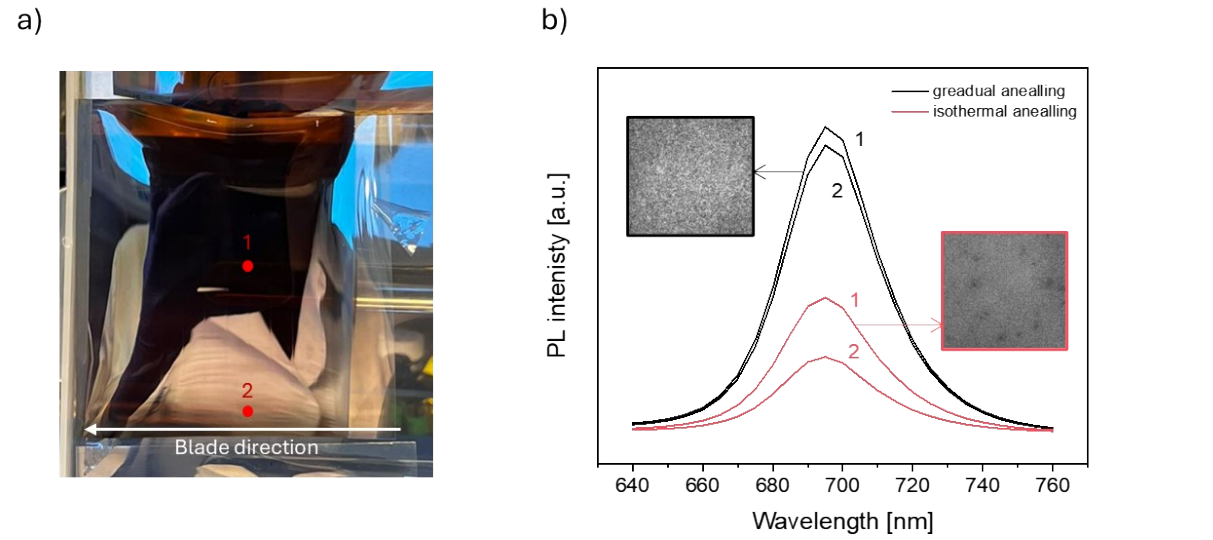

b) SEM images of the perovskite layer.

Figure S5. Photoluminescence characterization of the WBG perovskite films: a) picture of the representative sample with the two measurement positions indicated: center (1) and edge (2), b) ss-PL

spectra acquired at positions 1 and 2, together with the corresponding PL emission maps of the respective spots.

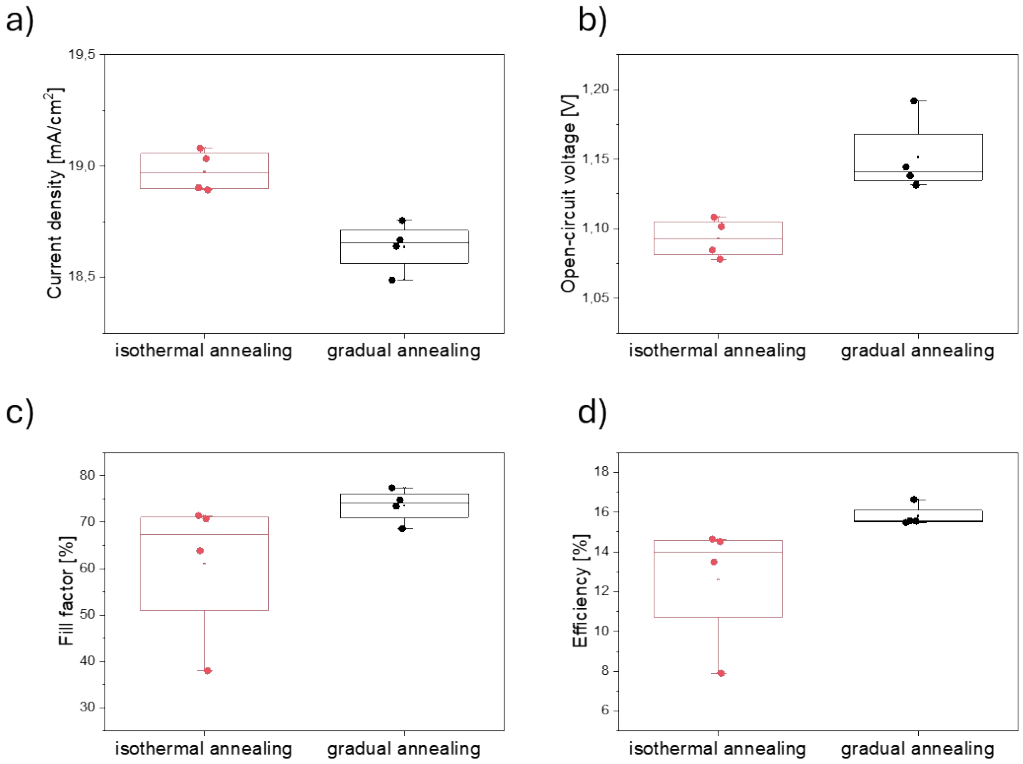

Figure S6. Impact of the annealing protocol on PV parameters of the solar cells. Comparison between gradual and isothermal annealing conditions.

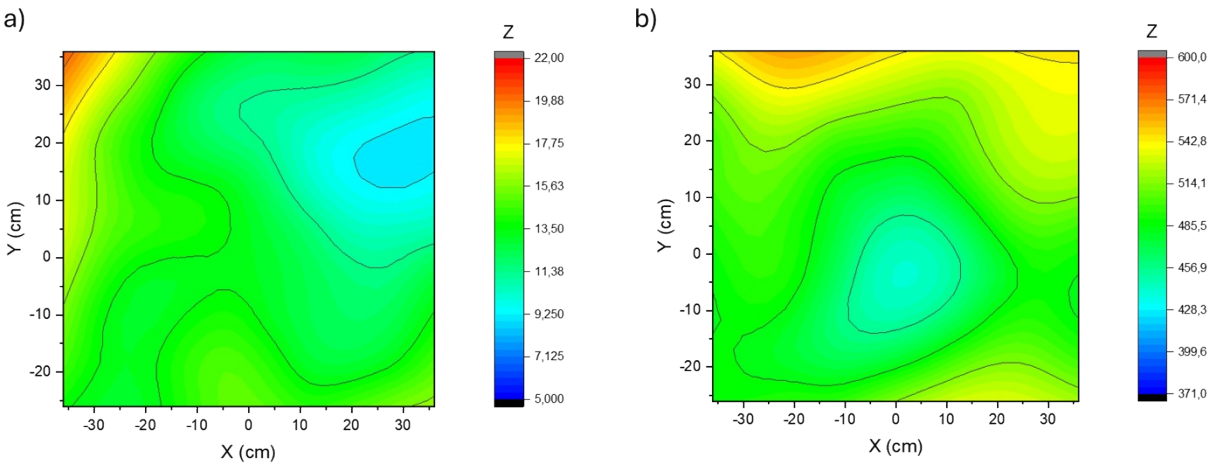

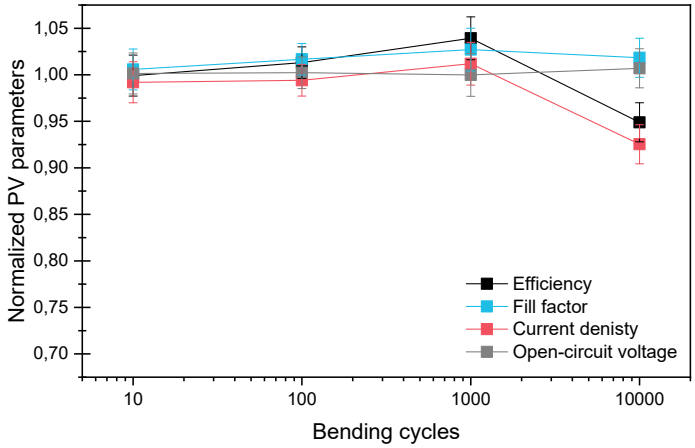

Figure S7. Ellipsometry thickness maps of a) NiOx and b) WBG perovskite layer.

Figure S8. Evolution of normalized PV parameters of WBG PSCs subjected to the bending test with a radius of 10 mm in ambient conditions.

Figure S9. Tauc plot of MBG perovskite of composition $Cs_{0.2}FA_{0.8}Pb(I_{0.90}Br_{0.10})_3$.

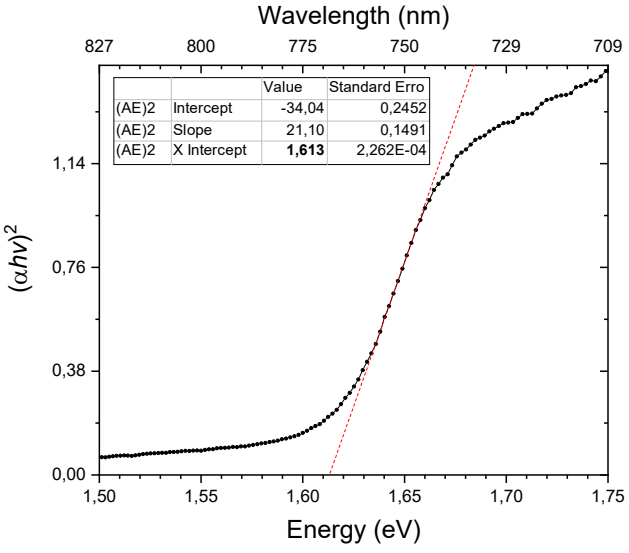

Figure S10. XRD diffractograms for WBG and MBG perovskite films. The broad background peak

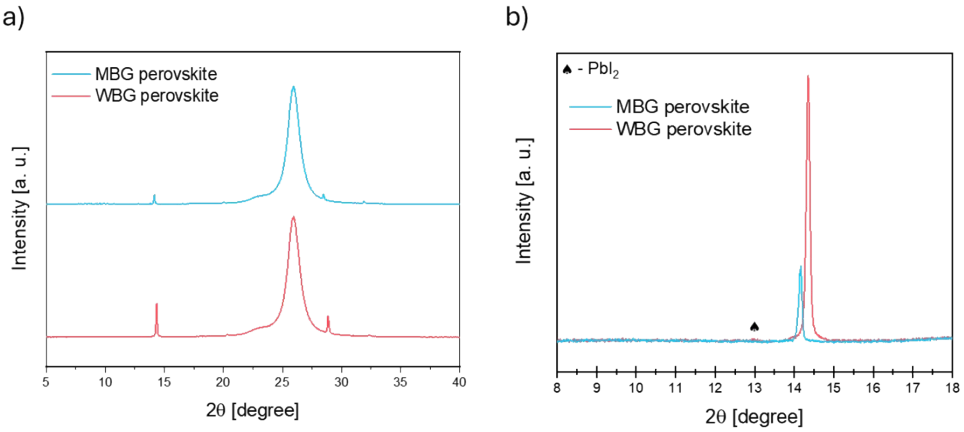

centred at approximately 25° 2θ originates from the amorphous PET substrate.

Figure S11. ss-PL spectrum for MBG and WBG perovskite absorbers.

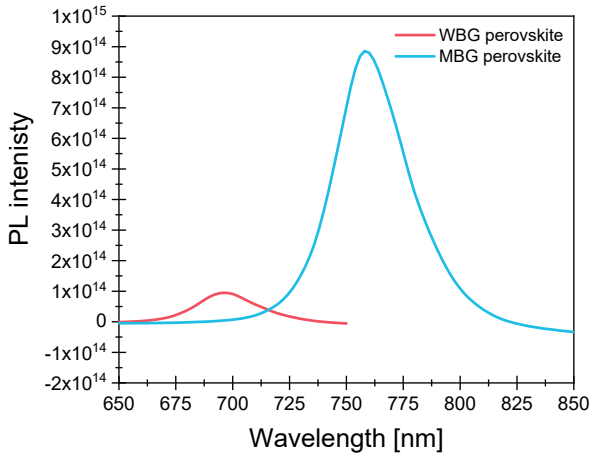

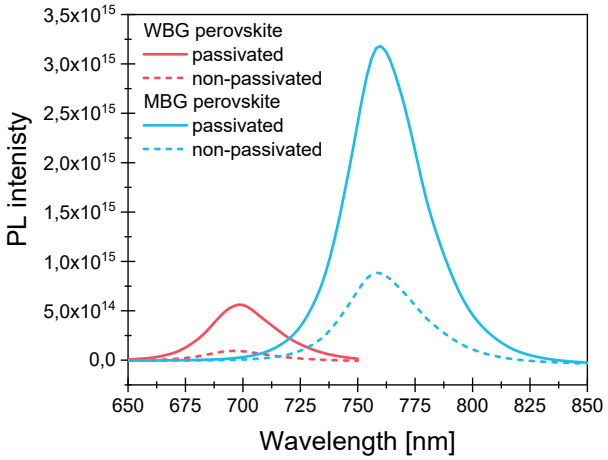

Figure S12. a) ss-PL intensity for passivated and non-passivated WBG and MBG perovskites.

Figure S13. Impact of passivation on statistics of open-circuit voltage of a) WBG perovskite, b) MBG perovskite solar cells.

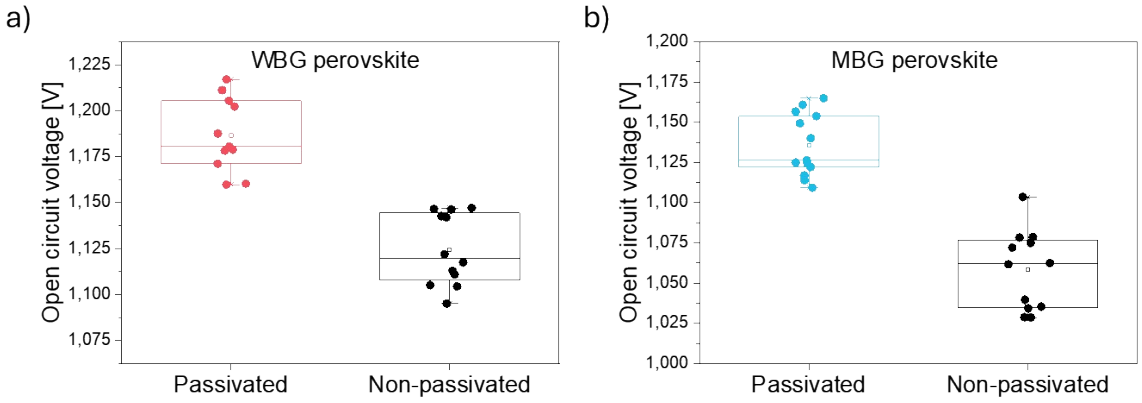

Figure S14. Power conversion efficiency (PCE) of inverted perovskite solar cells fabricated using scalable deposition methods on rigid and flexible substrates, plotted as a function of perovskite bandgap.[1-26]

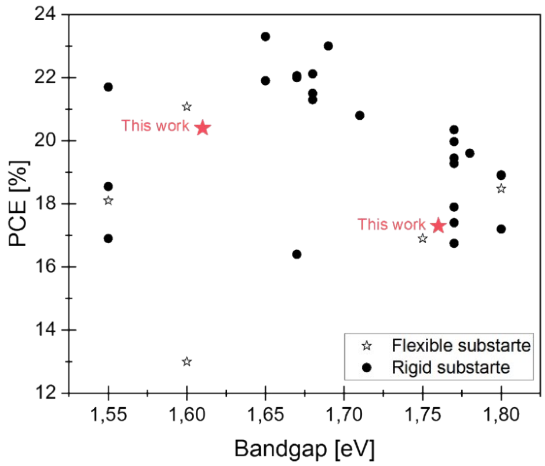

Table S1. State-of-the-art data reported for inverted perovskite solar cells and modules fabricated with the use of scalable deposition methods on polymeric foils: bandgap of the perovskite (E_g), efficiency of solar cell (PCE_C), efficiency of solar module (PCE_M), active area of the module (A_M), $\Delta PCE = ((PCE_C - PCE_M) / PCE_C \times 100\%)$. For consistent comparison, PCE_M was calculated on a per-active-area basis.

Deposition method	Eg [eV]	PCE_C [%]	PCE_M [%]	AA_M [cm^2]	ΔPCE [%]	Ref.
Blade-coating	1.51	23.4	19.8	9.4	15.4	[27]
Blade-coating	1.55	24.5	15.9	100	35.1	[28]
Blade-coating	1.58	21.1	16.9	14.6	20.0	[1]
Spray-coating	1.60	18.2	16.1	35	11.7	[4]
Blade-coating	1.60	13.0	10.5	15.7	19.2	[2]
Blade-coating	1.61	20.4	17.0	15.2	16.7	This work
Blade-coating	1.76	17.4	15.1	15.2	12.7	This work

Table S2. Summary of photovoltaic parameters extracted from the I-V measurements and MPPT tracking of laminated MBG PSMs.

Module	PCE_{scan} (%)	I_{SC} (mA)	V_{OC} (V)	FF (%)	PCE_{MPPT} (%)
1	12,9	-37,88	8,70	58,98	12,6
2	13,8	-36,65	8,93	63,83	13,3
3	13,4	-36,29	8,78	63,47	12,6
4	14,8	-38,63	9,03	64,37	14,6
5	13,7	-37,31	8,95	61,85	13,2

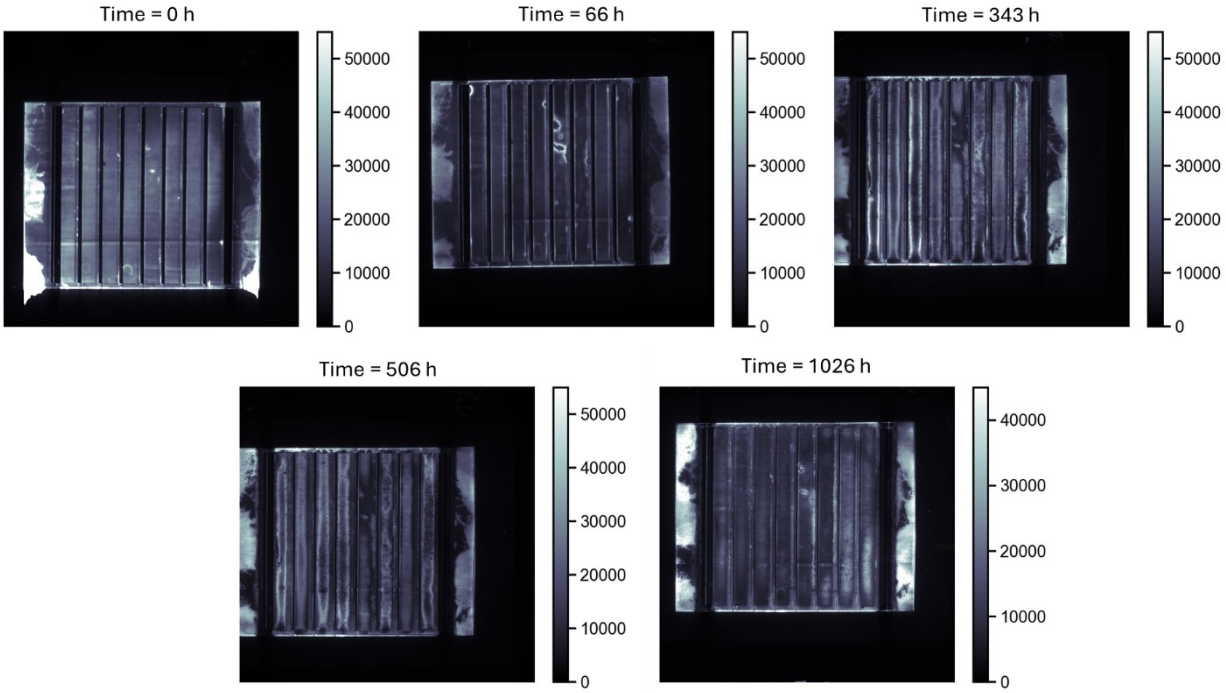

Figure S15. PL_{OC} maps of the encapsulated module recorded at 0, 66, 343, 506, and 1026 h of DH testing.

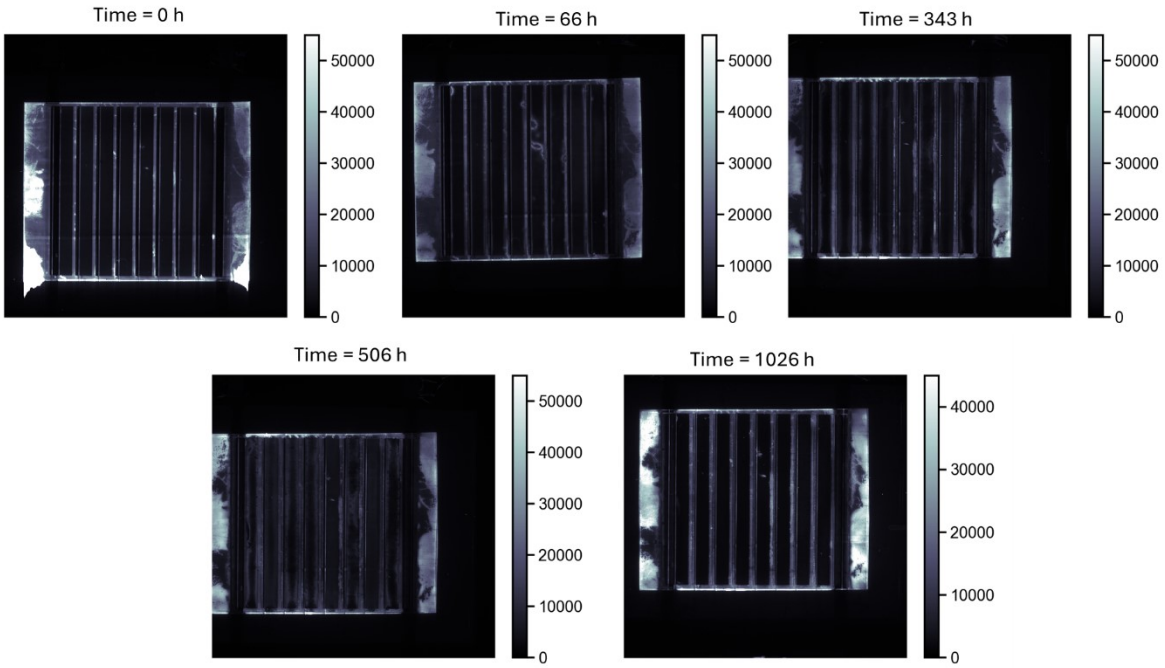

Figure S16. PL_{SC} maps of the encapsulated module recorded at 0, 66, 343, 506, and 1026 h of DH testing

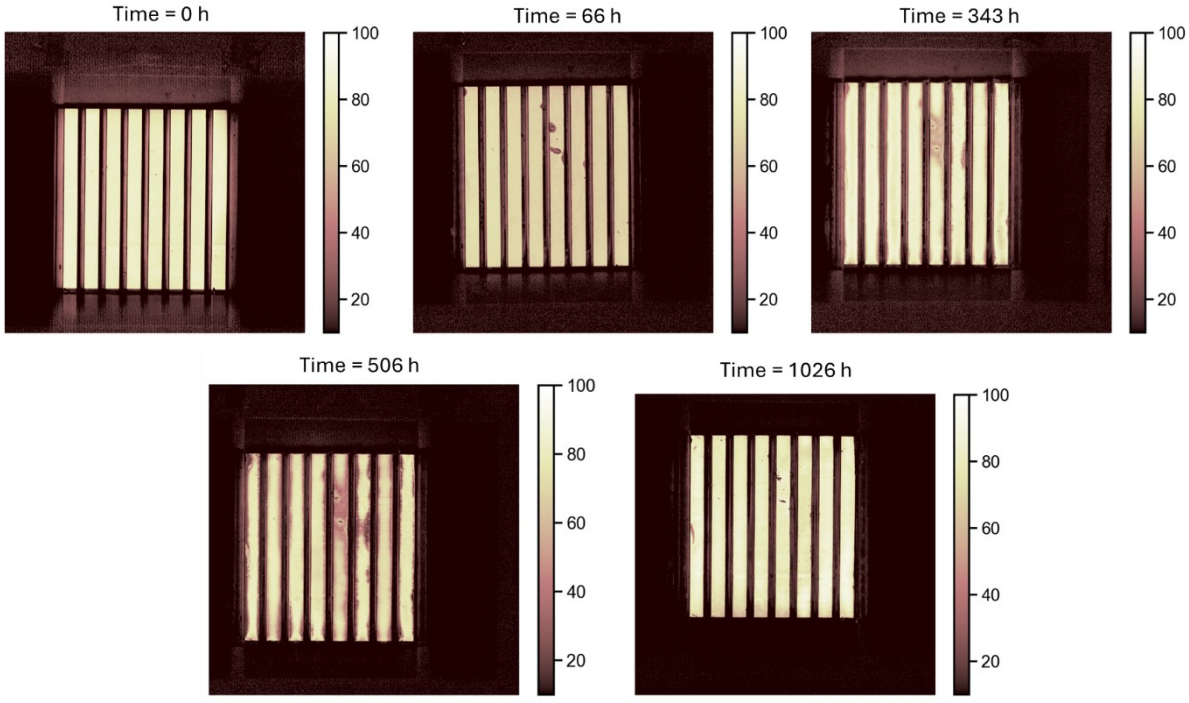

Figure S17. Extraction coefficient (EC) maps of the encapsulated module at 0, 66, 343, 506, and 1026 h of DH testing, where EC = $((PL_{OC} - PL_{SC})/PL_{OC})x100\%$.

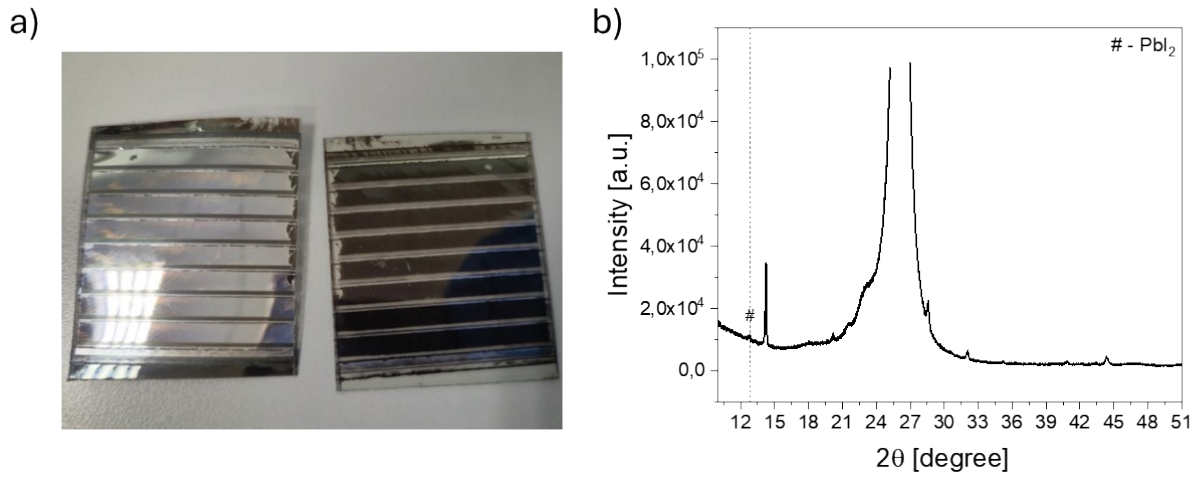

Figure S18. a) Picture of delaminated module after aging, b) XRD diffractograms of delaminated modules after aging. The broad background feature centred at approximately 25° 2θ originates from the amorphous substrate and encapsulation foils.

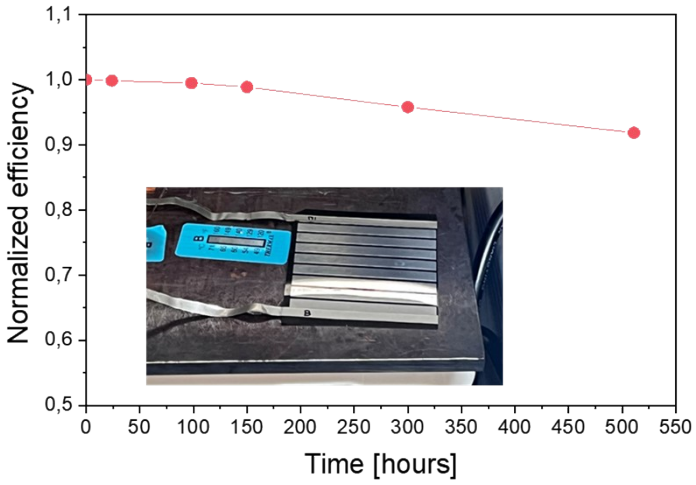

Figure S19. Evolution of normalized efficiency during thermal aging at 85 °C in a glovebox (nitrogen atmosphere) for modules featuring the same architecture as those used in the damp heat (DH) test.

Bibliography

1 B. Fan, J. Xiong, Y. Zhang, C. Gong, F. Li, X. Meng, X. Hu, Z. Yuan, F. Wang and Y. Chen, Adv. Mater., 2022, 34, 2201840.

2 L. A. Castriotta, R. Fuentes Pineda, V. Babu, P. Spinelli, B. Taheri, F. Matteocci, F. Brunetti, K. Wojciechowski and A. Di Carlo, ACS Appl. Mater. Interfaces, 2021, 13, 29576–29584.

3 Z. Hu, H. Cai, X. Luo, B. Han, J. Liu, Q. Guo, Y. Li, C. Liu, J. Ni, J. Li and J. Zhang, Small Methods, 2025, 9, 2402177.

4 M. Park, S. C. Hong, Y.-W. Jang, J. Byeon, J. Jang, M. Han, U. Kim, K. Jeong, M. Choi and G. Lee, Int. J. of Precis. Eng. and Manuf.-Green Tech., 2023, 10, 1223–1234.

5 L. Li, Y. Wang, X. Wang, R. Lin, X. Luo, Z. Liu, K. Zhou, S. Xiong, Q. Bao, G. Chen, Y. Tian, Y. Deng, K. Xiao, J. Wu, M. I. Saidaminov, H. Lin, C.-Q. Ma, Z. Zhao, Y. Wu, L. Zhang and H. Tan, Nat. Energy, 2022, 7, 708–717.

6 M. Li, H. Gao, L. Li, E. Wang, Z. Liu, I. T. Cheong, P. Wu, Y. Zhang, Y. Wang, X. Zheng, M. Yin, R. Lin, R. Liu, H. Luo, K. Xiao, W. Kong, W. Sun, Y. Nie, X. Luo, M. I. Saidaminov, Y. Li and H. Tan, Nat. Photonics, 2025, 19, 1255–1263.

7 P. Jia, G. Chen, G. Li, J. Liang, H. Guan, C. Wang, D. Pu, Y. Ge, X. Hu, H. Cui, S. Du, C. Liang, J. Liao, G. Xing, W. Ke and G. Fang, Adv. Mater., 2024, 36, 2400105.

8 X. Zhou, H. Lai, T. Huang, C. Chen, Z. Xu, Y. Yang, S. Wu, X. Xiao, L. Chen, C. J. Brabec, Y. Mai and F. Guo, ACS Energy Lett., 2023, 8, 502–512.

9 X. Dai, S. Chen, H. Jiao, L. Zhao, K. Wang, Z. Ni, Z. Yu, B. Chen, Y. Gao and J. Huang, Nat. Energy, 2022, 7, 923–931.

10 G. Yang, Z. Ni, Z. J. Yu, B. W. Larson, Z. Yu, B. Chen, A. Alasfour, X. Xiao, J. M. Luther, Z. C. Holman and J. Huang, Nat. Photonics, 2022, 16, 588–594.

11 Z. Liu, P. Wang, Y. Gao, X. Ge, Y. Luo, X. Du, S. Xu, B. Shi, S. Liu, Y. Zhao and X. Zhang, Adv. Funct. Mater., 2025, 35, 2510444.

12 J. Liu, M. Zhang, X. Sun, L. Xiang, X. Yang, X. Hu, Z. Wang, T. Hou, J. Qin, Y. Huang, M. Abdi-Jalebi and X. Hao, Nano-Micro Lett., 2025, 17, 318.

13 S. Fu, S. Zhou, W. Meng, G. Li, K. Dong, D. Pu, J. Zhou, C. Wang, H. Guan, W. Shao, L. Huang, Z. Su, C. Wang, G. Chen, P. Jia, J. Wang, Z. Xu, X. Gao, H. Cong, T. Wang, C. Xiao, G. Fang and W. Ke, Nat. Nanotechnol., 2025, 20, 764–771.

14 H. Fang, W. Shen, H. Guan, G. Chen, G. Li, W. Ai, S. Fu, Z. Xu, W. Chen, P. Jia, Z. Yu, S. Wang, Z. Yu, Q. Lin, J. Wang, W. Zheng, D. Pu, G. Fang and W. Ke, Adv. Mater., 2025, 37, 2414790.

15 K. Xiao, Y.-H. Lin, M. Zhang, R. D. J. Oliver, X. Wang, Z. Liu, X. Luo, J. Li, D. Lai, H. Luo, R. Lin, J. Xu, Y. Hou, H. J. Snaith and H. Tan, Science, 2022, 376, 762–767.

16 M. Yang, Z. Li, M. O. Reese, O. G. Reid, D. H. Kim, S. Siol, T. R. Klein, Y. Yan, J. J. Berry, M. F. A. M. van Hest and K. Zhu, Nat. Energy, 2017, 2, 17038.

17 C. Duan, H. Gao, K. Xiao, V. Yeddu, B. Wang, R. Lin, H. Sun, P. Wu, Y. Ahmed, A. D. Bui, X. Zheng, Y. Wang, J. Wen, Y. Wang, W. Ou, C. Liu, Y. Zhang, H. Nguyen, H. Luo, L. Li, Y. Liu, X. Luo, M. I. Saidaminov and H. Tan, Nat. Energy, 2025, 10, 318–328.

18 Y. Tang, Y. Zhang, X. Zhou, T. Huang, K. Shen, K. Zhang, X. Du, T. Shi, X. Xiao, N. Li, C. J. Brabec, Y. Mai and F. Guo, Nano Energy, 2023, 114, 108653.

19 D. Pu, X. Zhang, H. Fang, W. Shen, G. Chen, W. Chen, P. Jia, G. Li, H. Guan, L. Huang, Y. Zhou, J. Wang, W. Zheng, W. Meng, G. Fang and W. Ke, Sci. Adv., 2025, 11, eady3621.

20 G. Yang, H. Gu, J. Yin, C. Fei, Z. Shi, X. Shi, X. Ying and J. Huang, Nat. Sustain., 2025, 8, 456–463.

21 X. Ge, Z. Huang, Y. Gao, Z. Liu, B. Shi, P. Wang, S. Qi, J. Li, X. Du, S. Liu, Y. Zhao and X. Zhang, Adv. Funct. Mater., 2025, 35, 2503504.

22 X. Ge, Z. Huang, B. Shi, P. Wang, Z. Liu, Y. Gao, X. Du, Y. Zhao and X. Zhang, Adv. Funct. Mater., 2025, 35, 2417493.

23 D. Pu, S. Zhou, H. Guan, P. Jia, G. Chen, H. Fang, S. Fu, C. Wang, H. Hushvaktov, A. Jumabaev, W. Meng, X. Wang, G. Fang and W. Ke, Adv. Funct. Mater., 2024, 34, 2314349.

24 Q. Xiao, A. Zhang, W. Ye, X. Yang, Y. Zhu, B. Jiang, C. Ge, X. Li, H. Song, C. Chen and J. Tang, Sol. RRL, 2023, 7, 2300486.

25 H. Gao, K. Xiao, R. Lin, S. Zhao, W. Wang, S. Dayneko, C. Duan, C. Ji, H. Sun, A. D. Bui, C. Liu, J. Wen, W. Kong, H. Luo, X. Zheng, Z. Liu, H. Nguyen, J. Xie, L. Li, M. I. Saidaminov and H. Tan, Science, 2024, 383, 855–859.

26 A. Jaffrès, M. Othman, F. Saenz, A. Hessler-Wyser, Q. Jeangros, C. Ballif and C. M. Wolff, ACS Appl. Mater. Interfaces, 2024, 16, 36557–36566.

27 W. Xu, B. Chen, Z. Zhang, Y. Liu, Y. Xian, X. Wang, Z. Shi, H. Gu, C. Fei, N. Li, M. A. Uddin, H. Zhang, L. Dou, Y. Yan and J. Huang, Nat. Photonics, 2024, 18, 379–387.

28 C. Gong, C. Wang, X. Meng, B. Fan, Z. Xing, S. Shi, T. Hu, Z. Huang, X. Hu and Y. Chen, Adv. Mater., 2024, 36, 2405572.